Photoacoustics 14 (2019) 31–36

Contents lists available at ScienceDirect

Photoacoustics

journal homepage: www.elsevier.com/locate/pacs

Research article

# Photoacoustic-based oxygen saturation assessment of murine femoral bone marrow in a preclinical model of leukemia

Cayla Wood[a,c], Karine Harutyunyan[b], Diego R.T. Sampaio[d], Marina Konopleva[b,c], Richard Bouchard[a,c,*]

[a] Department of Imaging Physics, The University of Texas MD Anderson Cancer Center, Houston, TX 77030, USA
[b] Department of Leukemia, The University of Texas MD Anderson Cancer Center, Houston, TX 77030, USA
[c] The University of Texas MD Anderson Cancer Center UTHealth Graduate School of Biomedical Sciences, Houston, TX 77030, USA
[d] Department of Physics, University of Sao Paulo, Ribeirao Preto, SP, Brazil

ARTICLE INFO

*Keywords:*
Photoacoustic imaging
Acute lymphoblastic leukemia
$SO_2$ estimation
Bone marrow
Preclinical imaging

ABSTRACT

A variety of hematological diseases manifest in the bone marrow (BM), broadly characterized as BM failure (BMF). BMF can be caused by acute lymphoblastic leukemia (ALL), which results in an expansion of hypoxic regions in the BM. Because of this hypoxic presentation, there is potential for improved characterization of BMF through *in vivo* assessment of oxygenation in the BM cavity. Photoacoustic (PA) imaging can provide local assessment of intravascular oxygen saturation ($SO_2$), which has been shown to correlate with pimonidazole-assessed hypoxia. This study introduces an optimized PA imaging technique to assess $SO_2$ within the femoral BM cavity through disease progression in a murine model of ALL. Results show a statistically significant difference with temporal changes in $SO_2$ (from baseline) between control and diseased cohorts, demonstrating the potential of PA imaging for noninvasive, label-free monitoring of BMF diseases.

## 1. Introduction

A variety of hematological diseases manifest in the bone marrow (BM), broadly characterized as BM failure (BMF), defined as an abnormality in erythroid, megakaryocytic, and monocyte cell lineages [1,2]. In some cases, BMF can be caused by acute lymphoblastic leukemia (ALL), in which ALL cells engraft in BM, leading to hypoxia-inducible factor 1-alpha (HIF-1α) induction in the BM niche [3,4]. This results in an expansion of hypoxic regions, which allows leukemic cells to infiltrate further, compromising normal hematopoietic cells [5]. Consequently, diagnosis and treatment of many hematological diseases stand to benefit from accurate characterization of BMF through assessment of *in vivo* oxygenation in the BM.

Current clinical methods to probe hypoxia, which is a lack of oxygen availability to cells, include ($^{18}$F-FAZA)-PET imaging, BOLD-MRI, TOLD-MRI, and $^{19}$F-MRI. ($^{18}$F-FAZA)-PET imaging has shown correlation with hypoxia immunostaining [6]; however, it requires injection of a radiotracer and suffers from inherently poor spatiotemporal resolution. BOLD-MRI is a label-free technique that suffers from quantitation issues, particularly at tissue-bone interfaces, due to susceptibility artifacts [7,8]. Although not affected by such artifacts, TOLD-MRI's limited sensitivity has failed to provide substantial signal change in BM [9,10]. $^{19}$F-MRI requires a perfluorocarbon exogenous reporter and additional imaging equipment that is not standard on an MRI scanner to generate dynamic $pO_2$ maps [11,12]. Preclinical methods to detect intracellular hypoxia include histological techniques (e.g., pimonidazole immunohistochemistry) and multiphoton intravital microscopy to probe carbonic anhydrase IX, a direct HIF-1α target [13,14]. However, these techniques require an exogenous agent and are generally limited to sampling a single time-point [15]. To date, there is no established method for *in vivo*, label-free, noninvasive, quantitative imaging of oxygenation in BM.

Photoacoustic (PA) imaging is a noninvasive, label-free, *in vivo* imaging technique with high spatiotemporal resolution that provides optical contrast at significantly greater depths than purely optical techniques [16,17]. Intravascular oxygen saturation ($SO_2$) can be estimated through PA-based assessment of oxy- and deoxyhemoglobin ($HbO_2$ and HHb, respectively) [18]. Although $SO_2$ is not a direct measure of intracellular hypoxia, it has been shown to be correlated with pimonidazole-assessed hypoxia and $pO_2$ levels proximal to capillaries [19,20]. Therefore, we hypothesize that $SO_2$ can serve as a noninvasive and label-free biomarker for leukemic disease progression and treatment response. This work demonstrates an optimized longitudinal PA imaging technique to probe the oxygenation status of the

* Corresponding author at: Department of Imaging Physics, The University of Texas MD Anderson Cancer Center, Houston, TX 77030, USA.
*E-mail address:* RRBouchard@mdanderson.org (R. Bouchard).

https://doi.org/10.1016/j.pacs.2019.01.003
Received 7 November 2018; Received in revised form 18 January 2019; Accepted 24 January 2019
Available online 20 February 2019

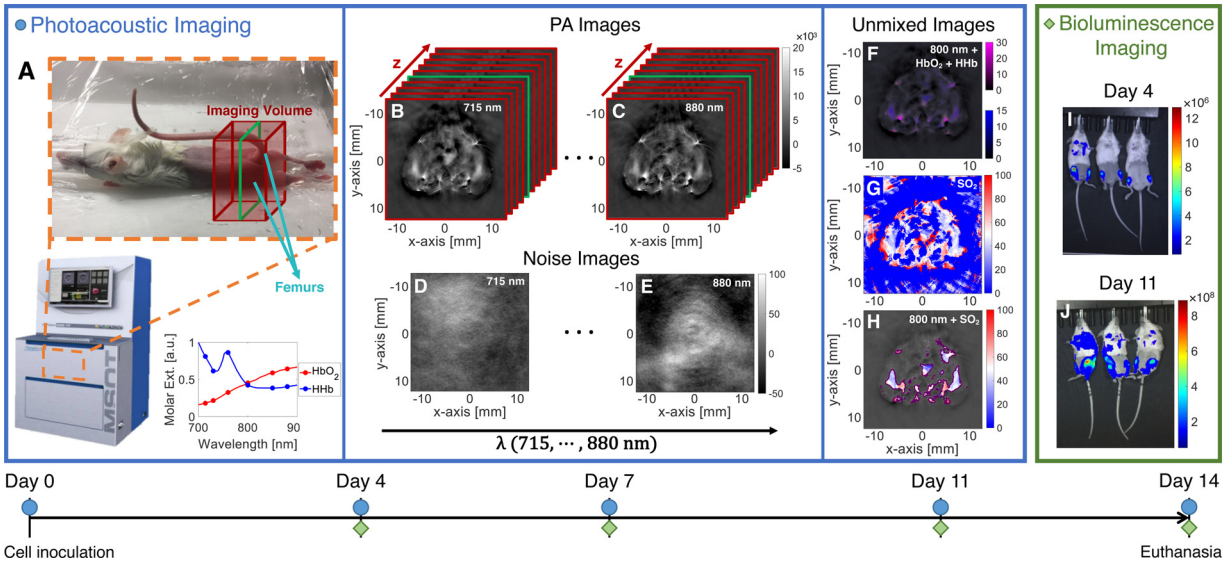


**Fig. 1.** (A) Setup for PA imaging in MSOT inVision 256-TF. Mice are positioned as shown in orange dashed box, then placed in the scanner for imaging. Scan range is set to include the extent of both femurs (red volume; middle imaging frame indicated by green outline). Wavelengths were selected based on the $HbO_2$ and HHb extinction spectra, as shown. Volume stack of PA images with corresponding noise images at (B),(D) 715 nm and (C),(E) 880 nm. Unmixed axial images with (F) $HbO_2$ and HHb overlaid 800-nm image and (G) $SO_2$ image. (H) SNR-masked $SO_2$ image overlaid 800-nm image. Matched BLI at (I) day 4 and (J) day 11, showing increase in cell engraftment in femurs as disease progresses. Timeline at the bottom shows imaging time-points, with PA imaging indicated by blue circles and BLI indicated by green diamonds.

femoral BM. Results from a preclinical pilot study show that temporal changes in intrafemoral $SO_2$ correlate with ALL disease progression.

## 2. Materials and methods

### 2.1. Mouse model

All animal work was performed in accordance with a protocol approved by the Institutional Animal Care and Use Committee. A transgenic murine leukemic BM cell (LBC) line was generated from murine Ai14/CD19-Cre BM B-cells that express TdTomato [13]. These cells were retrovirally transduced with the p190/Bcr-Abl oncogene and grown in cell culture for transduction with the Luciferase retrovirus [13]. $2 \times 10^5$ LBCs were then suspended in PBS and inoculated intravenously into six- to eight-week-old B6-albino mice (Jackson Laboratory, Bar Harbor, ME). Engraftment was confirmed with bioluminescence imaging (BLI) at least 2 days post-injection (Fig. 1).

### 2.2. Imaging acquisition

All PA imaging was performed on the MSOT inVision 256-TF imaging system (iThera Medical, Munich, DEU), which has a 256-element, 270°-arc acoustic-receiver array with 5 laser-fiber-bundle pairs for PA signal generation. Images are acquired axially (Fig. 1B–C), and the mouse is translated in the z-axis to obtain volumetric data. The wavelengths used in this study included 715, 730, 760, 800, 850, and 880 nm; at least 10 frame-averages were used for all acquisitions. Water temperature was maintained at 34 °C; mice were anesthetized with 1.2% isoflurane delivered via 100% oxygen at a flow rate of 0.8 L/min. Fur was removed with Nair prior to imaging, and a thin layer of ultrasound gel was applied to improve acoustic coupling.

Measures were taken to ensure repeatability of animal setup between imaging sessions. For the first time-point, the mouse was positioned with its hind limbs in the ankle cuffs and extended as far as reasonable (Fig. 1A). This position was recorded to place the mouse in the same location at subsequent time-points. Mice were imaged over a 25 mm volume with a 0.2 mm step size, resulting in a scan time around 12 min; the scan volume included the full extent of both femurs, with extra frames superior and inferior to ensure the entire femur was sampled.

After all PA data were acquired, images were reconstructed by iterative reconstruction using the ViewMSOT software package (v.3.8, iThera Medical). Images were then unmixed for $HbO_2$ and HHb using linear regression, and voxel-wise $SO_2$ was calculated as the ratio of $HbO_2$ to total hemoglobin [21]. Unless otherwise stated, reported $SO_2$ values are defined as the average within a region of interest (ROI) encompassing the noted anatomy (i.e., intra-ROI mean).

### 2.3. CT/PA co-registration

To verify that observed PA signals originated in the femoral BM, control mice were imaged on both the MSOT and the AlbiraSi X-ray CT (Bruker, Billerica, MA) imaging systems, verifying matched animal positioning with anatomical fiducials. 3D PA image data were then manually co-registered with 3D X-ray CT image data to determine whether the hemoglobin signal visible in PA images co-located with the BM cavity. Additionally, a noise threshold was applied to PA images to verify that only pixels with signal-to-noise ratio (SNR) > 6 dB were included in analysis [22].

### 2.4. System characterization

To determine the optimal imaging parameters, it was necessary to balance scan time with $SO_2$ estimation precision. Scan time increases linearly with wavelength number and frame-averaging; precision tends to maintain a nonlinear relationship with these parameters. Imaging-wavelength combinations (table, Fig. 3) were assessed with 10-, 15-, and 20-frame averages in a wild-type ("control") mouse. Optimization was then determined based on the minimum of a cost function:

$$CF = \sigma \times nAvg^2, \quad (1)$$

where σ is the standard deviation in femoral-artery $SO_2$ ($S_aO_2$) estimates (to assess measurement precision) and nAvg is the number of employed frame-averages (weighted more heavily to minimize scan time for noticeably frail leukemic mice). To obtain σ, four axial locations were imaged using parameters detailed in 2.2. $S_aO_2$ was obtained

from an ROI encompassing the femoral artery; σ was then calculated as the standard deviation of $S_aO_2$ across the axial locations. The femoral artery was selected for this analysis because it is a known value (i.e., the mouse is breathing 100% $O_2$, so we expect $S_aO_2$ near 100%) and is a clear anatomical marker in PA images.

Based on this optimization, three controls were imaged over five time-points (timeline, Fig. 1) with six wavelengths and 15-frame averaging. Femoral-BM $SO_2$ ($S_fO_2$) was obtained from ROIs placed over femoral- BM signals in 800-nm axial PA images. $S_fO_2$ for each mouse was assessed over the length of the femur ("femoral extent") for all five time-points; intra-ROI standard deviation was also calculated to ensure that ROI placement was correct. Then, to compare $S_fO_2$ across all controls, the intra-cohort mean and standard deviation ($S_f\bar{O}_2$ and $\sigma_{S_fO_2}$, respectively) were assessed over the femoral extent for all time-points.

### 2.5. Leukemia pilot study

A pilot study was performed to compare temporal differences in $S_f\bar{O}_2$ between control and leukemic mice through disease progression. Five mice were inoculated with LBCs, as described in 2.1 ("leukemic"); three were not injected ("controls"). Each mouse was imaged at five time-points: pre-inoculation, and days 4, 7, 11, and 14 post-inoculation. Controls were imaged as described in 2.4; leukemic mice were imaged similarly with six wavelengths, but with 10-frame averaging to reduce imaging time for the frail leukemic cohort. BLI was performed at each post-inoculation time-point to track leukemic cell engraftment. $S_f\bar{O}_2$ and $\sigma_{S_fO_2}$ were compared between cohorts at each time-point; statistical significance was determined by a two-tailed *t*-test ($\alpha = 0.05$). Additionally, absolute changes in $S_fO_2$ were assessed relative to baseline for each mouse, and the intra-cohort mean of these changes ($|\Delta S_f\bar{O}_2|$; e.g., $|S_f\bar{O}_2^{\,Day11} - S_f\bar{O}_2^{\,Day0}|$) was assessed; statistical significance was determined by a two-way repeated measures ANOVA ($\alpha = 0.05$). Day 14 results were excluded from analysis because leukemic mice had experienced paralysis and > 10% loss in body mass, which significantly confounded $S_fO_2$ measurements.

## 3. Results and discussion

### 3.1. CT/PA co-registration

Co-registered PA and CT images of a control mouse demonstrate colocalization of the femoral PA (i.e., hemoglobin) signal and the CT-delineated BM cavity (Fig. 2C). The BM PA signal appears diffuse due to intra-cavity sound reverberation. Additionally, the applied SNR threshold helped to better delineate the femoral-BM PA signal (Fig. 2D).

### 3.2. System characterization

Optimized wavelength/averaging combinations were determined based on minima of the cost function (Eq. (1)), which selected 6-wavelength unmixing and either 10- or 15-frame averaging (red circles, Fig. 3A). Using these parameters, control mice were imaged over five time-points to assess temporal variability of $S_f\bar{O}_2$. The average of $S_f\bar{O}_2$ estimates across the femoral extent and all time-points was 46.1 ± 1.0%. Spatial dependence in $S_fO_2$ is evident across the femoral extent: $S_fO_2$ tends to increase towards the distal end (Fig. 3B,C). This could be attributed to differences in depths of femoral-BM PA signals as there is more soft tissue surrounding the proximal end than the distal end. Varying depths could affect the accuracy of $HbO_2$ and HHb unmixing (due to wavelength-dependent optical attenuation [18]) and therefore change the calculated $S_fO_2$. However, day-to-day $S_fO_2$ estimates in each frame showed less than 2.4% $S_fO_2$ variation in each subject, implying that this effect is temporally stable and thus allows for longitudinal assessment of other factors, such as disease progression.

### 3.3. Leukemia pilot study

At day 0 in the leukemic cohort, $S_f\bar{O}_2$ averaged over the femoral extent was 45.8%; at day 11, this reduced to 36.8%. Additionally, leukemic $\sigma_{S_fO_2}$ averaged over the femoral extent increased from 5.2% at day 0 to 10.2% at day 11 (shaded regions, Fig. 4). Neither of these changes was statistically significant. As BM hypoxia increases, the expectation would be for $S_fO_2$ to decrease; however, as demonstrated by the high $\sigma_{S_fO_2}$ at day 11, some leukemic mice experienced increased $S_fO_2$ with disease progression relative to baseline, while others experienced decreased $S_fO_2$. This indicates that although hypoxia and $S_fO_2$ are correlated, they are not directly related. $S_fO_2$ assesses vascular oxygenation, whereas hypoxia exists further downstream in the extravascular compartment and can be caused by a variety of biological effects (i.e., abnormalities in vasculature or sufficient diffusion distance [23]), which cannot be discerned from $S_fO_2$ assessment alone.

Fig. 5 shows plots of $|\Delta S_f\bar{O}_2|$ across the femoral extent. Statistical significance was assessed separately in three regions: the proximal end, the femoral body, and the distal end. There was a statistically significant difference in $|\Delta S_f\bar{O}_2|$ between the leukemic and control cohorts in the femoral body region (asterisks, Fig. 5). Therefore, it may be necessary to measure subject-specific temporal changes in $S_fO_2$ to be sensitive to changes in leukemic disease progression.

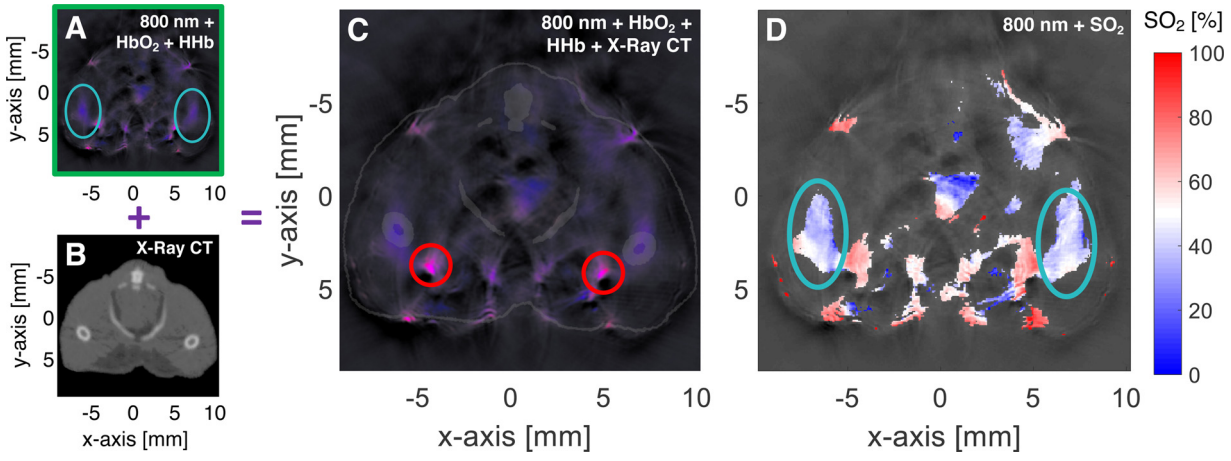


**Fig. 2.** (A) Axial PA image in a representative mouse showing 800-nm background (grayscale) with $HbO_2$ (red) and HHb (blue) unmixed overlay with signal from femoral BM (indicated by teal circles); (B) matched X-ray CT to show anatomy. (C) Overlay of X-ray CT on PA image shows that the hemoglobin signal seen in the PA image co-locates with the BM cavity seen on X-ray CT, indicating that the signal originated in the BM. Femoral arteries are indicated by red circles. (D) SNR-masked $SO_2$ image overlaid on 800-nm PA image demonstrates that sufficient SNR is achieved in the BM cavity to reliably estimate femoral $SO_2$.

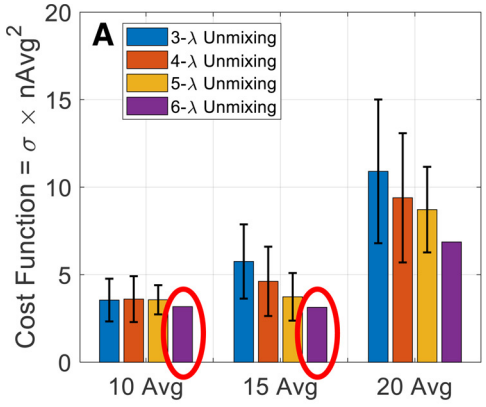


| Wavelength Combinations | | | |
|---|---|---|---|
| 3 λ | 4 λ | 5 λ | 6 λ |
| 715, 760, 800 | 715, 760, 800, 850 | 715, 730, 760, 800, 850 | 715, 730, 760, 800, 850, 880 |
| 715, 760, 850 | 715, 760, 800, 880 | 715, 730, 760, 800, 880 | |
| 715, 760, 880 | 715, 760, 850, 880 | 715, 830, 760, 850, 880 | |
| 715, 800, 850 | 715, 800, 850, 880 | 715, 760, 800, 850, 880 | |
| 715, 800, 880 | 730, 760, 800, 850 | 730, 760, 800, 850, 880 | |

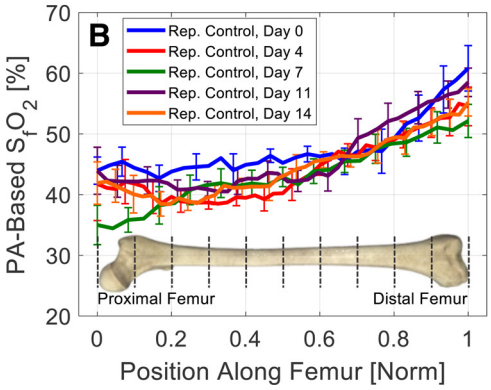


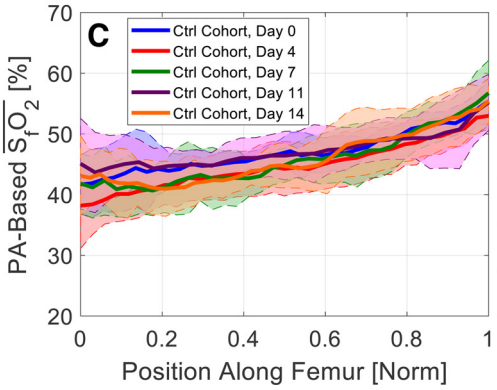


| Day | Average $\overline{S_fO_2}$ |
|---|---|
| 0 | 47.0±3.4% |
| 4 | 44.8±3.9% |
| 7 | 45.8±4.5% |
| 11 | 47.2±2.8% |
| 14 | 45.9±4.2% |

**Fig. 3.** (A) Plot of cost function for all tested acquisition parameters. Wavelength combinations are shown in the table on the top right. PA-based (B) $S_fO_2$ for a representative control mouse and (C) $S_f\bar{O}_2$ for control cohort. The average $S_f\bar{O}_2$ across the femoral extent for all time-points are summarized in the table on the bottom right.

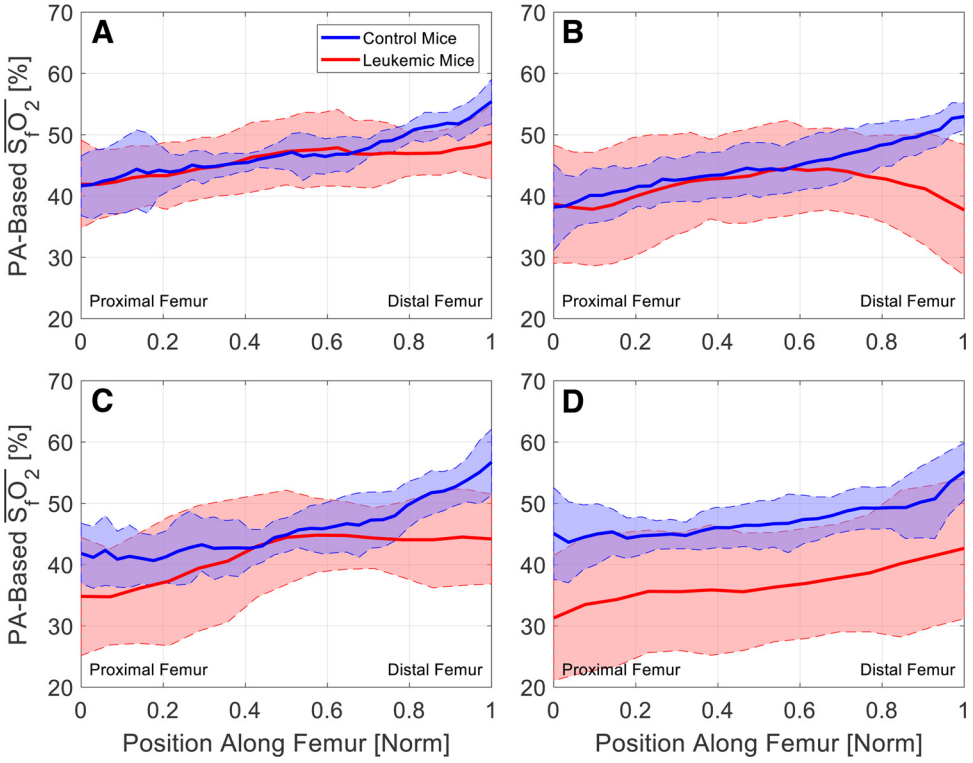


**Fig. 4.** PA-based femoral $SO_2$ for control (blue) and leukemic (red) mice at (A) day 0, (B) day 4, (C) day 7, and (D) day 11. Each line shows $S_f\bar{O}_2$ for the cohort, and shaded regions indicate $\sigma_{S_fO_2}$ for the cohort.

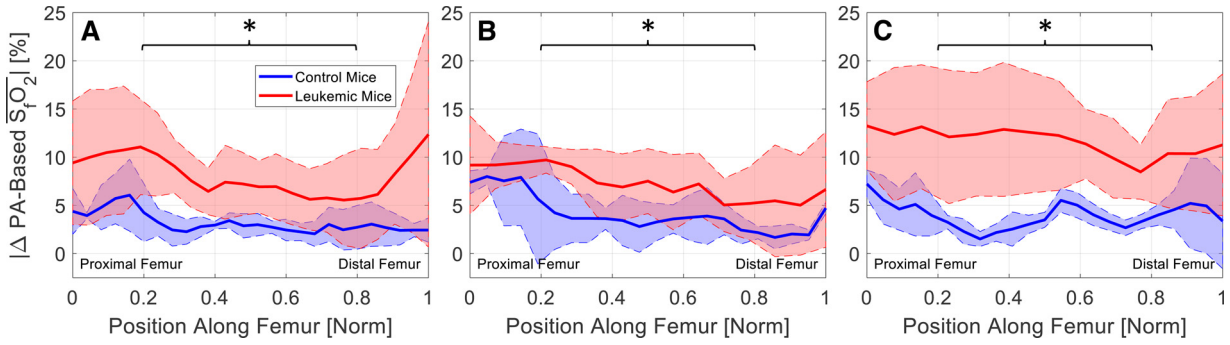


**Fig. 5.** $|\Delta S_f\bar{O}_2|$ for (A) day 4 – day 0, (B) day 7 – day 0, and (C) day 11 – day 0. There is a statistically significant difference between controls (blue) and leukemic (red) mice in the middle region of the femur, as indicated by * (Repeated Measures Two-Way ANOVA; $\alpha = 0.05$), between leukemic and control cohorts.

In future studies, contrast may be further improved by varying oxygen inhalation conditions (e.g., 100% and 21% $O_2$), a method that has been demonstrated in other disease models [24]. Additionally, $S_fO_2$ measurements at the final time-point could be correlated with hypoxia through immunohistochemical analysis, which is established for this disease model [13]. These studies will help further discern the relationship between $|\Delta S_f\bar{O}_2|$ and leukemic disease progression. PA-based $S_fO_2$ assessment could, in turn, be used as a preclinical assay to assess the efficacy of novel ALL treatments currently under investigation [25]. Furthermore, this assay could be applied to a variety of BMF applications, particularly aplastic anemia, in which there is a reduction in hematopoietic production [2]. Although clinical PA-based measurements in BM may be difficult, some sites (e.g., appendages) could be imaged with an arc-array, which offers an increased receive angle for improved sensitivity [26]. This would be particularly applicable to pediatric patients, whose bones are thinner and more readily permit one-way transmission of PA-generated US signal out of the BM cavity [27,28].

## 4. Conclusions

This work presents an optimized *in vivo*, noninvasive, label-free PA imaging technique for $S_fO_2$ estimation, demonstrating a repeated-measure variability of less than 2.4% in a control cohort. This technique was applied to a pilot cohort of leukemic mice, and temporal changes in $S_fO_2$ demonstrated a statistically significant correlation with leukemic disease progression. PA-based $S_fO_2$ imaging is able to reliably assess changes in BM oxygenation status, an emerging imaging biomarker that has potential to provide valuable insight into many hematological diseases that manifest as BMF.

## Author statement

**Cayla Wood:** Methodology, Software, Formal Analysis, Investigation, Writing – Original Draft, Writing – Review & Editing.

**Karine Harutyunyan:** Methodology, Resources, Writing – Review & Editing.

**Diego Sampaio:** Software, Formal Analysis.

**Marina Konopleva:** Supervision, Funding Acquisition, Writing – Review & Editing.

**Richard Bouchard:** Conceptualization, Supervision, Writing – Review & Editing.

## Acknowledgements

This work is supported by the National Institute of Health [S10 OD019946, R01 CA155056, P30 CA016672]. The authors would like to thank Jorge De La Cerda, Caterina Kaffes, and Charles Kingsley for their help with animal preparation; Niki Zacharias Millward and Sriram Shanmugavelandy for their assistance with BLI acquisitions; and Seth Gammon and Jingfei Ma for insightful discussions about analysis of the model.

## References

[1] D. Bodine, N. Berliner, Introduction to the review series on “bone marrow failure, Blood 124 (2014) 2755.
[2] A. Shimamura, Clinical approach to marrow failure, Am. Soc. Hematol. Educ. Prog. 2009 (2009) 329–337.
[3] C.-H. Pui, Encyclopedia of Cancer, Springer, Berlin Heidelberg, 2011.
[4] N. Baran, M. Konopleva, Molecular pathways: hypoxia-activated prodrugs in cancer therapy, Clin. Cancer Res. 23 (2017) 2382–2390.
[5] J. Benito, M.S. Ramirez, N.Z. Millward, J. Velez, K.G. Harutyunyan, H. Lu, Y.X. Shi, P. Matre, R. Jacamo, H. Ma, S. Konoplev, T. McQueen, A. Volgin, M. Protopopova, H. Mu, J. Lee, P.K. Bhattacharya, J.R. Marszalek, R.E. Davis, J.A. Bankson, J.E. Cortes, C.P. Hart, M. Andreeff, M. Konopleva, Hypoxia-activated prodrug TH-302 targets hypoxic bone marrow niches in preclinical leukemia models, Clin. Cancer Res. 22 (2016) 1687–1698.
[6] G.B. Halmos, L.B. De Bruin, Ja. Langendijk, B.Fa.M. van der Laan, J. Pruim, R.J.H.M. Steenbakkers, Head and neck tumor hypoxia imaging by 18F-fluoroazomycin-arabinoside (18F-FAZA)-PET, Clin. Nucl. Med. 39 (2014) 44–48.
[7] J.A. Detre, J. Wang, Technical aspects and utility of fMRI using BOLD and ASL, Clin. Neurophysiol. 113 (2002) 621–634.
[8] Y. Ding, R.P. Mason, R.W. McColl, Q. Yuan, R.R. Hallac, R.D. Sims, P.T. Weatherall, Simultaneous measurement of tissue oxygen level-dependent (TOLD) and blood oxygenation level-dependent (BOLD) effects in abdominal tissue oxygenation level studies, J. Magn. Reson. Imaging 38 (2013) 1230–1236.
[9] S. Remmele, R.P. Mason, J.P.B. O'Connor, MRI hypoxia measurements, in: A. Luna, J. Vilanova, L. Hygino da Cruz, JrS. Rossi (Eds.), Funct. Imaging Oncol. Springer, Berlin Heidelberg, 2014, pp. 269–289.
[10] E. Tadamura, H. Hatabu, W. Li, P.V. Prasad, R.R. Edelman, Effect of oxygen inhalation on relaxation times in various tissues, J. Magn. Reson. Imaging 7 (1997) 220–225.
[11] S.R. Thomas, R.G. Pratt, A.J. McGoron, R.C. Samaratunga, R.W. Millard, Monitoring P02 in bone marrow using perfluorocarbon F-19 NMR, ISMRM Conf. Proc. (1998).
[12] M.E. Bellemann, J. Brückner, P. Peschke, G. Brix, R.P. Mason, Quantification and visualization of oxygen partial pressure in vivo by19f NMR imaging of perfluorocarbons, Biomed. Technol. 47 (2002) 451–454.
[13] K.G. Harutyunyan, F. Nwajei, M.A. Zal, D.A. Fruman, S. Mallampati, X. Sun, T. Zal, M. Konopleva, The dynamics of stroma-leukemia interaction in the hypoxic BM niches in vivo, Blood 124 (2014) 2396.
[14] K.H. Shin, J.A. Diaz-Gonzalez, J. Russell, Q. Chen, P. Burgman, X.F. Li, C.C. Ling, Detecting changes in tumor hypoxia with carbonic anhydrase IX and pimonidazole, Cancer Biol Ther. 6 (2007) 70–75.
[15] B.M. Seddon, D.J. Honess, B. Vojnovic, G.M. Tozer, P. Workman, Measurement of tumor oxygenation: in vivo comparison of a luminescence fiber-optic sensor and a polarographic electrode in the p22 tumor, Radiat. Res. 155 (2001) 837–846.
[16] R.R. Bouchard, O. Sahin, S.S. Emelianov, Ultrasound-guided photoacoustic imaging: current state and future development, IEEE Trans. Ultrason. Ferroelectr. Freq. Control. 61 (2014) 450–466.
[17] T. Mitcham, K. Dextraze, H. Taghavi, M. Melancon, R. Bouchard, Photoacoustic imaging driven by an interstitial irradiation source, Photoacoustics 3 (2015) 45–54.
[18] T. Mitcham, H. Taghavi, J. Long, C. Wood, D. Fuentes, W. Stefan, J. Ward, R. Bouchard, Photoacoustic-based SO2 estimation through excised bovine prostate tissue with interstitial light delivery, Photoacoustics 7 (2017) 47–56.
[19] M. Gerling, Y. Zhao, S. Nania, K.J. Norberg, C.S. Verbeke, B. Englert, R.V. Kuiper, Å. Bergström, M. Hassan, A. Neesse, J.M. Löhr, R.L. Heuchel, Real-time assessment of tissue hypoxia in vivo with combined photoacoustics and high-frequency ultrasound, Theranostics 4 (2014) 604–613.
[20] Y. Wang, S. Hu, K. Maslov, Y. Zhang, Y. Xia, L.V. Wang, In vivo integrated photoacoustic and confocal microscopy of hemoglobin oxygen saturation and oxygen partial pressure, Opt. Lett. 36 (2011) 1029–1031.
[21] K. Maslov, H.F. Zhang, L.V. Wang, Effects of wavelength-dependent fluence attenuation on the noninvasive photoacoustic imaging of hemoglobin oxygen

saturation in subcutaneous vasculature in vivo, Inverse Probl. 23 (2008) S113–S122.
[22] M.A. Naser, D.R.T. Sampaio, N.M. Munoz, C.A. Wood, T.M. Mitcham, W. Stefan, K.V. Sokolov, T.Z. Pavan, R. Avritscher, R.R. Bouchard, Improved photoacoustic-based oxygen saturation estimation with SNR-regularized local fluence correction, IEEE Trans. Med. Imaging 0062 (2018) 1–11.
[23] P. Vaupel, A. Mayer, Hypoxia in cancer: significance and impact on clinical outcome, Cancer Metastasis Rev. 26 (2007) 225–239.
[24] M.R. Tomaszewski, I.Q. Gonzalez, J.P.B. O'Connor, O. Abeyakoon, G.J.M. Parker, K.J. Williams, F.J. Gilbert, S.E. Bohndiek, Oxygen enhanced optoacoustic tomography (OE-OT) reveals vascular dynamics in murine models of prostate cancer, Theranostics 7 (2017) 2900–2913.
[25] F. Chiarini, A. Lonetti, C. Evangelisti, F. Buontempo, E. Orsini, C. Evangelisti, A. Cappellini, L.M. Neri, J.A. McCubrey, A.M. Martelli, Advances in understanding the acute lymphoblastic leukemia bone marrow microenvironment: from biology to therapeutic targeting, Biochim. Biophys. Acta 1863 (2015) 449–463.
[26] R.A. Kruger, C.M. Kuzmiak, R.B. Lam, D.R. Reinecke, S.P. Del Rio, D. Steed, Dedicated 3D photoacoustic breast imaging, Med. Phys. 40 (2013) 113301.
[27] C.Y. Wu, C.C. Glüer, M. Jergas, E. Bendavid, H.K. Genant, The impact of bone size on broadband ultrasound attenuation, Bone 16 (1995) 137–141.
[28] E. Schönau, Problems of bone analysis in childhood and adolescence, Pediatr. Nephrol. 12 (1998) 420–429.

**Cayla A. Wood** received her B.S. degree in Engineering Physics in 2014 and her M.S. degree in Applied Physics in 2015, both from Colorado School of Mines. She is currently a doctoral candidate at the University of Texas MD Anderson Cancer Center UTHealth Graduate School of Biomedical Sciences where she is pursuing a Ph.D. in Medical Physics. Her research interests include preclinical and clinical photoacoustic imaging for diagnostics and therapy guidance.

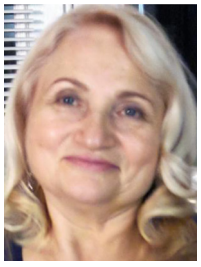

**Karine G. Harutyunyan** received her Ph.D. degree from the Institute of Developmental Biology in Moscow, Russia. She completed post-graduate training at Baylor College of Medicine. She is currently a Research Scientist in Dr. Konopleva's lab in the Department of Leukemia at the University of Texas MD Anderson Cancer Center. She generates novel mouse models for HIF-1α-deficient ALL for the investigation of hypoxia and metabolism in leukemia models.

**Diego R.T. Sampaio** received his B.Sc. degree in Medical Physics in 2012 and his M.Sc. degree in Physics Applied to Medicine and Biology in 2014, both from the University of São Paulo, Brazil. He is currently a doctoral candidate at the University of São Paulo where he is pursuing a Ph.D. in Physics Applied to Medicine and Biology. His research interests include ultrasound, magneto-motive ultrasound, and photoacoustic imaging.

**Marina Y. Konopleva** received her M.D. degree from Pavlov Medical School and her Ph.D. from the Institute of Hematology in St. Petersburg, Russia. She completed a post-graduate internship and specialty training and joined the Section of Molecular Hematology and Therapy at the University of Texas MD Anderson Cancer Center in 1996. She is currently a Professor of Medicine in the Department of Leukemia at MD Anderson Cancer Center. Her research interests include novel therapies for patients with acute leukemia and targeting apoptosis, hypoxia, and metabolism.

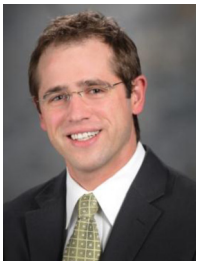

**Richard R. Bouchard** received his B.S. degree in Biomedical and Electrical engineering and Cultural Anthropology from Duke University in 2004 and received his Ph.D. degree in Biomedical engineering from Duke University in 2010. He completed a postdoctoral fellowship in the Ultrasound Imaging and Therapeutics Research Laboratory at the University of Texas at Austin in 2012. Dr. Bouchard is currently an Assistant Professor in the Department of Imaging Physics at the University of Texas MD Anderson Cancer Center. His research interests include preclinical and clinical photoacoustic-ultrasonic imaging and ultrasound-based elasticity imaging.